

Ultrafast electron microscopy in material science

Huaixin Yang(杨槐馨), Shuaishuai Sun(孙帅帅), Ming Zhang(张明), Zhongwen Li(李中文), Zian Li(李子安), Peng Xu(徐鹏), Huanfang Tian(田焕芳), Jianqi Li(李建奇)

Citation: Chin. Phys. B . 2018, 27(7): 070703. **doi:** 10.1088/1674-1056/27/7/070703

Journal homepage: http://cpb.iphy.ac.cn; http://iopscience.iop.org/cpb

What follows is a list of articles you may be interested in

Ultrafast electron diffraction

Xuan Wang(王瑄), Yutong Li(李玉同)

Chin. Phys. B . 2018, 27(7): 076102. **doi:** 10.1088/1674-1056/27/7/076102

Power flow analysis in a hybrid phononic crystal structure

Hanbei Guo(郭寒贝), Qiang Li(李强), Liubin Zhou(周刘彬), Lei Qiang(强磊)

Chin. Phys. B . 2018, 27(3): 036302. **doi:** 10.1088/1674-1056/27/3/036302

Complete low-frequency bandgap in a two-dimensional phononic crystal with spindle-shaped inclusions

Ting Wang(王婷), Hui Wang(王辉), Mei-Ping Sheng(盛美萍), Qing-Hua Qin(秦庆华)

Chin. Phys. B . 2016, 25(4): 046301. **doi:** 10.1088/1674-1056/25/4/046301

Two-coupled structural modulations in charge-density-wave state of $SrPt_2As_2$ superconductor

Wang Li, Wang Zhen, Shi Hong-Long, Chen Zhen, Chiang Fu-Kuo, Tian Huan-Fang, Yang Huai-Xin, Fang Ai-Fang, Wang Nan-Lin, Li Jian-Qi

Chin. Phys. B . 2014, 23(8): 086103. **doi:** 10.1088/1674-1056/23/8/086103

Surface segregation of InGaAs films by the evolution of reflection high-energy electron diffraction patterns

Zhou Xun,Luo Zi-Jiang,Guo Xiang,Zhang Bi-Chan,Shang Lin-Tao,Zhou Qing,Deng Chao-Yong,Ding Zhao

Chin. Phys. B . 2012, 21(4): 046103. **doi:** 10.1088/1674-1056/21/4/046103

TOPICAL REVIEW — Synergetic Extreme Condition User Facility: Breakthroughs and opportunities for the research of physical science

Ultrafast electron microscopy in material science*

Huaixin Yang(杨槐馨)[1,2], Shuaishuai Sun(孙帅帅)[1], Ming Zhang(张明)[1,2], Zhongwen Li(李中文)[1,2], Zian Li(李子安)[1], Peng Xu(徐鹏)[1], Huanfang Tian(田焕芳)[1], and Jianqi Li(李建奇)[1,2,3,†]

[1] *Beijing National Laboratory for Condensed Matter Physics, Institute of Physics, Chinese Academy of Sciences, Beijing* 100190, *China*
[2] *School of Physical Sciences, University of Chinese Academy of Sciences, Beijing* 100049, *China*
[3] *Collaborative Innovation Center of Quantum Matter, Beijing* 100084, *China*

(Received 3 April 2018; revised manuscript received 12 May 2018; published online 25 June 2018)

Recent advances in the ultrafast transmission electron microscope (UTEM), with combined spatial and temporal resolutions, have made it possible to directly visualize the atomic, electronic, and magnetic structural dynamics of materials. In this review, we highlight the recent progress of UTEM techniques and their applications to a variety of material systems. It is emphasized that numerous significant ultrafast dynamic issues in material science can be solved by the integration of the pump–probe approach with the well-developed conventional transmission electron microscopy (TEM) techniques. For instance, UTEM diffraction experiments can be performed to investigate photoinduced atomic-scale dynamics, including the chemical reactions, non-equilibrium phase transition/melting, and lattice phonon coupling. UTEM imaging methods are invaluable for studying, in real space, the elementary processes of structural and morphological changes, as well as magnetic-domain evolution in the Lorentz TEM mode, at a high magnification. UTEM electron energy-loss spectroscopic techniques allow the examination of the ultrafast valence states and electronic structure dynamics, while photoinduced near-field electron microscopy extends the capability of the UTEM to the regime of electromagnetic-field imaging with a high real space resolution.

Keywords: ultrafast transmission electron microscope (UTEM), structural dynamics, electron diffraction, ultrafast imaging

PACS: 07.78.+s, 61.05.J–, 63.20.–e, 64.70.–p **DOI:** 10.1088/1674-1056/27/7/070703

1. Introduction

Pump–probe-based time-resolved experiments attract considerable attention owing to their capability of providing time-domain information regarding the characteristics/strengths of the couplings between structural, electronic, and spin degrees of freedom by following the dynamic response of a system to pulsed excitation.[1,2] By employing diverse probe pulses, the evolution of different microscopic or macroscopic properties of the excited systems can be measured. Pump–probe-based time-resolved spectroscopic experiments using visible, infrared, and ultraviolet (UV) light can be used to map the evolution of electronic states up to a time resolution of several femtoseconds.[3,4] Ultrafast x-ray techniques, particularly the x-ray free-electron laser[1,2,5,6] and electron diffraction,[1,7] are fast-growing and can be used to track the lattice dynamics with femtosecond temporal resolution. UTEM, which combines femtosecond temporal resolution with the excellent imaging, diffraction, and spectroscopy capabilities of conventional transmission electron microscopy (TEM) owing to the well-developed state-of-the-art electron optics, promises to become one of the most powerful experimental tools for the investigation of ultrafast dynamics on the nanoscale.[7] Inspired by pioneering works at the Technical University Berlin,[8] California Institute of Technology (Caltech),[9] and Lawrence Livermore National Labs (LLNL),[10] time-resolved electron microscopy, both the stroboscopic[7] and single-shot methods,[10] has been currently extensively explored in a growing number of laboratories worldwide. We successfully developed a UTEM at the Institute of Physics, Chinese Academy of Sciences (IOP, CAS) in 2014.[11]

Over the past few years, the UTEM has been developed through the integration of different microscopic techniques, including imaging modes (bright-field (BF) and dark-field (DF) imaging, high-resolution TEM (HRTEM), scanning TEM (STEM), Lorentz TEM (LTEM), energy-filtered TEM (EFTEM), and tomography) and diffraction modes (selected-area electron diffraction with parallel electron beams, convergent-beam electron diffraction (CBED), electron energy-loss spectroscopy (EELS), and photoinduced near-field electron microscopy (PINEM)), which has introduced significant opportunities to solve fundamental problems in physics, materials science, chemistry, and biology. UTEMs have been used to study elementary struc-

*Project supported by the National Basic Research Program of China (Grant No. 2015CB921300), the National Key Research and Development Program of China (Grant Nos. 2016YFA0300300, 2017YFA0504703, and 2017YFA0302900), the National Natural Science Foundation of China (Grant Nos. 11604372, 11474323, and 11774391), the "Strategic Priority Research Program (B)" of the Chinese Academy of Sciences (Grant No. XDB07020000), and the Scientific Instrument Developing Project of the Chinese Academy of Sciences (Grant No. ZDKYYQ20170002). Z. A. L acknowledges the financial support of the Hundred Talent Program B from CAS.

†Corresponding author. E-mail: ljq@iphy.ac.cn

© 2018 Chinese Physical Society and IOP Publishing Ltd

tural changes during photoinduced chemical reactions, non-equilibrium structural phase transitions/melting, the crystallization of solids, and nanoscale elastic deformations with a combination of Ångstrom-scale spatial resolution and femtosecond/picosecond time resolution. These results provide unprecedented insight into the non-equilibrium transformation pathways. The development and applications of the UTEM in materials science and biology have been extensively reviewed.[1,7,9,10,12–31]

Herein, we first provide a conceptual design of the UTEM and illustrate the detailed design of the UTEM of our research group at the Institute of Physics. Then, a brief overview of the literature is presented, with a focus on the results obtained by our group. Specific cases are discussed to demonstrate the utility of the different UTEM techniques in materials science with unprecedented real-time and real-space capabilities.

2. Principle of UTEM

The UTEM is reformed on the basis of a commercial transmission electron microscope, and the time-resolution function is realized by introducing an ultrafast laser via the pump–probe technique.[7,10,30] As shown in Fig. 1(a), a probe laser irradiates the photocathode to generate pulsed photoelectron through the photoelectric effect, and a pump laser irradiates the sample and initiates the ultrafast process. After a specific time delay between the pump and probe lasers, an ultrafast electron pulse reaches the sample, recording the sample state at this time through diffraction, imaging, or spectroscopy using the classic TEM signal-detection system. By changing the time delay Δt, the dynamic process is revealed. The hardware modification of the conventional transmission electron microscope generally involves the incorporation of two side-mounted sub-laser systems providing proper optics for precisely aligning laser pulses on a photoelectron source in the gun and onto a region of interest in the specimen.

In view of the different needs of the experiment, there are two experimental models: the stroboscopic mode and the single-shot mode.[7,10,30] As shown in Fig. 1(b), each pulse in the stroboscopic mode contains 1–10^3 electrons, and each pulse in the single-shot mode contains 10^6–10^8 electrons.

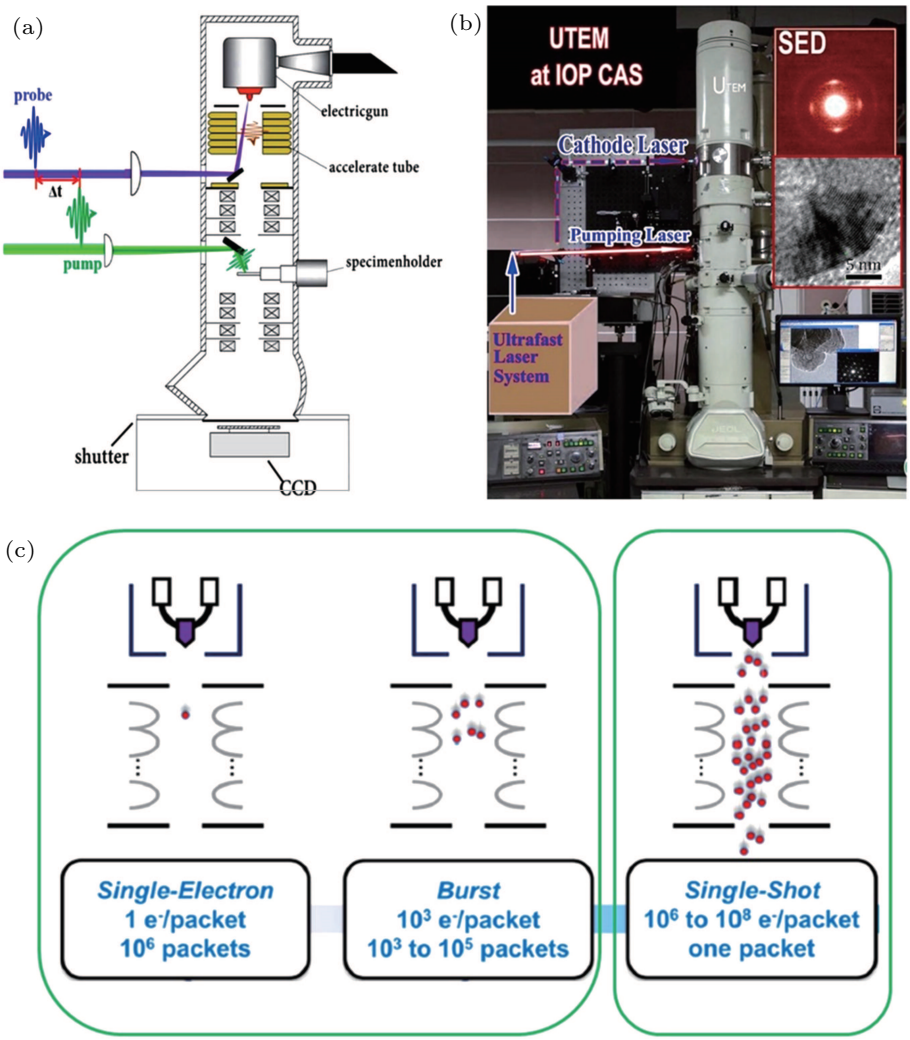


Fig. 1. (color online) Schematic of the UTEM and the two typical experimental modes. (a) Simplified schematic of the UTEM experimental layout. (b) Electron dose in a single pulse for the stroboscopic mode (left) and the single-shot mode (right) (modified from Ref. [35], Fig. 1(a)). (c) Ultrafast electron microscope in our lab at the Institute of Physics. The UTEM is based on a JEOL EX2000 200-kV thermionic transmission electron microscope.

The most significant difference between the two experimental modes is the number of electronic pulses required to obtain a single image. The stroboscopic mode requires the stacking of multiple electronic pulses in order to satisfy the electron dose required for a single image. As a limit, there is at most one electron in each pulse of the stroboscopic mode, eliminating the pulse broadening caused by the space-charge effect due to the Coulomb repulsion in the electron packet. The single-electron stroboscopic imaging concept, which can yield the optimum time-resolution, was first proposed and realized by Zewail *et al.*[7] Generally, the stroboscopic mode can be applied to phenomena that are reversible at timescales commensurate with or shorter than the temporal interval set by the laser repetition rate (e.g., nanoseconds to milliseconds). The single-shot mode needs only a single photoelectron pulse containing many electrons to achieve the electron dose required for a single image and can thus be applied to study the irreversible dynamics. Because of the high current densities, the spatial and temporal coherence are sacrificed to some extent for ensuring that the microscope can still form images. In the fields of chemistry and biology, many biochemical processes are irreversible, and the ultrafast electron microscope single-shot mode can capture the important events in an irreversible process and then—through the replacement of the regional experiments—the whole dynamic process can be restored. The single-shot mode was first achieved by LLNL, and the movie mode was developed to record one irreversible process by deflecting nine successive electron pulses to different areas of the camera with adjustable time intervals.[10]

3. Development of UTEM at Institute of Physics

After the pioneering work of Zewail of Caltech and the research work of LLNL, there are some groups in the worldwide established thermal-emission TEM-based UTEM setup, such as Carbone *et al.* at EPFL,[32,33] Flannigan *et al.* in Minnesota,[31] Banhart *et al.* in France,[34] Kwon *et al.* at UNIST of Korea,[35] and other research groups at the KTH Royal Institute of Technology, Sweden,[36] and Russia.[37] These UTEMs are based on a thermionic gun (LaB_6 cathode) with a Wehnelt electrode and can be operated in the nanosecond, single-shot, femtosecond, and single/few-electron modes. The Wehnelt bias and the cathode–Wehnelt distance significantly influence the temporal and energy spreads of the picosecond electron pulses, which are determined by the space-charge and Boersch effects, according to the number of electrons in a pulse.[36,38–41]

To obtain the dynamic structural features with high time and spatial resolutions, we developed a UTEM at the Institute of Physics, Chinese Academy of Sciences (IOP, CAS) in 2014,[11] as shown in Fig. 1(c). Previously, research groups at LLNS and Caltech modified the TEM column structure by introducing an electron-shift Cu block between the anode and the condenser lens. Moreover, a weak magnetic lens was added in their UTEM to increase the number of electrons for time-resolved observations.[9,10] Our UTEM was constructed via the modification of a 200-kV electron gun on a JEOL-2000EX microscope. The electronic configuration and vacuum systems were re-designed and improved, as shown in Fig. 1(a). Additionally, our UTEM includes a femtosecond laser system. As shown in the figure, the ultrafast laser system equipped with this UTEM is used to pump samples and generate electron pulses for stroboscopic observations. The pump and probe lasers are generated from the same laser source (Spirit 1040-4, Spectra-Physics), with repetition ranging from a single shot to 1 MHz. The output wavelength is 1040 nm, and the maximum pulse energy is > 40 μJ. Generally, the output laser is split into two parts: one for sample pumping after second-harmonic generation (520 nm) and another for the probe laser after third-harmonic generation (347 nm). The pump laser is focused onto an area as small as 60 μm for UTEM observations. The probe laser is focused onto an area of 100 μm to match the size of the cathode.

Before performing UTEM pump–probe measurements, we adjust our laser/TEM system and calibrate the synchronization between the pumping femtosecond laser and the electron-pulse probe with sub-picosecond precision. The electron-shadow image of surface plasma is used to determine the time zero. The Cu TEM grid is excited by the pump laser at the center to generate a plasma cloud, which pushes the probe electron pulses away from the Cu grid, as shown in Fig. 2(a). Figure 2(b) shows the normalized changes (measured according to the root-mean-square (RMS)) of the signal difference as a function of the time delay. The time zero can be evidently determined at the onset of the plasma-cloud formation. The temporal resolution of UTEM images is essentially limited by space-charge effects and certain ultrashort processes that cannot be observed. To investigate the space charge broadening effects and the duration of the photoelectron pulse resulting from the alteration of the cathode laser, we performed measurements (on both UTEM images and diffraction patterns) with the fluence of the probe laser between 10 μJ/cm^2 and 10 mJ/cm^2. The results clearly indicate that the probe electron pockets can be strongly broadened by space-charge effects for laser fluences larger than 1 mJ/cm^2. To reduce the space-charge broadening effect for a high temporal resolution, we decreased the number of electrons to one or a few tens in each pocket by reducing the probe-laser power. If there are a few tens of electrons in a single pulse, the duration of the photoelectron pulse is approximately 1 ps, according to previous theoretical calculations and experimental measurements.

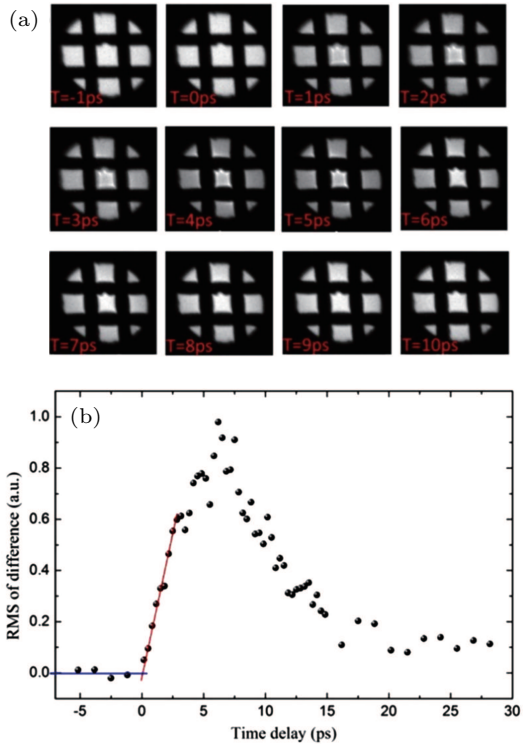


Fig. 2. (color online) (a) Time evolution of an electron image for a Cu grid excited by femtosecond pump laser pulses. (b) Normalized changes (measured according to the RMS) of the signal difference as a function of the time delay. Reprinted from Ref. [11] with permission.

Temperature accumulation is a common phenomenon in high-repetition rate pump–probe experiments owing to the laser-induced heating effect. For the stroboscopic mode, it is important to check the signal difference between the laser-on (negative delay) and laser-off states to determine whether there is obvious temperature accumulation. The time constant of the recovery process can be determined by reducing the repetition rate in the pump–probe experiments, by replacing the probe laser with a nanosecond UV laser, and using a digital delay generator to tune the time delay between the pump laser and the probe electron beam at the timescale of nanoseconds to micro- or milliseconds. Usually, the time constant of the thermal-dominated recovery process can vary from microseconds to milliseconds depending on the condition of thermal dissipation. To assist the recovery process and avoid heat accumulation, a supporting grid with a large mesh number and high thermal conductivity (e.g., coated with C nanotubes), along with a pump laser having a small beam size, is often used.

4. Applications of UTEM in materials science

UTEM techniques have been successfully used to study the ultrafast evolutions of atomic and electronic rearrangements under non-equilibrium conditions in organic, inorganic, and biological materials.[7,10,19,22,27,29] In this section, we provide a short review of the application of the UTEM in materials science, separately addressing the information obtained in the reciprocal (diffraction), real (imaging), and energy (spectroscopy) spaces.

4.1. Applications of ultrafast electron diffraction of UTEM

Diffraction techniques (neutrons, x-rays, and electrons) are classic methods for determining the atomic structure. For the concept of pump–probe experiments, although pulsed x-ray sources with high brightness are realized in large-scale facilities, such as free-electron lasers or synchrotrons, laboratory-scale x-ray experiments suffer from comparably low photon numbers.[1,7] Owing to the large scattering cross section of electrons, it is possible to perform time-resolved electron-diffraction experiments using very compact laboratory-scale setups.[1] Via TEM diffraction, Bragg spots, Debye–Scherrer rings, and CBED diffraction patterns can be obtained for different types of samples with parallel or convergent electron beams. By analyzing the position, intensity, or width of the spots/ring/lines, information regarding the structural dynamics can be obtained. For example, thermal heating, no thermal effects, phase transitions, coherent lattice vibrations, and lattice phonon coupling can be analyzed according to the intensity/scattering vector change of particular diffraction peaks; the variation of the scattering vector for the observed Bragg reflections can be used for the study of the nanoscale energy transport, electron–phonon coupling, and lattice relaxation at the picosecond timescale.[7,10,31] When convergent-beam illumination is adopted, the transverse (shear) dynamics of certain lattice planes can be directly probed.[42] Spatially focused and timed electron packets of UTEM CBED allow the determination of structures in three dimensions with highly precise localization, showing potential for investigating dynamic processes of single particles and structures of heterogeneous media.

Here, we highlight two of our recent works to demonstrate the capability of the ultrafast electron diffraction (UED) mode of the UTEM.

4.1.1. Ultrafast structural dynamics of multi-walled nanotubes

High spatial resolution of the UTEM is ideal for dynamical studies of nanostructured materials with an inherently small volume or mass. Previous results demonstrate that UTEM can be used for the study of nanoscale energy transport, phase transitions, chemical reaction, electron–phonon coupling, and lattice relaxation at the picosecond timescale.[7,10,11,31,43–45]

Our previous work on the ultrafast structural dynamics of multi-walled C nanotubes clearly revealed the strong anisotropic nature of the lattice dynamics, showing that distinguishable lattice relaxations appear in intra-tubular sheets at an ultrafast timescale of a few picoseconds, followed by lattice expansion along the radial direction.[11] This anisotropic

feature is fundamentally correlated with the specific tubular structure and chemical bonding behaviors, i.e., the strong covalent bonds in the tubular sheet and the weak van der Waals inter-layer bonds along the radial direction.

We recently investigated the ultrafast structural dynamics of multi-walled boron nitride nanotubes (BNNTs) under femtosecond optical excitation using the UED mode of the UTEM.[46] Analysis of the time-resolved (100) and (002) diffraction profiles reveals the highly anisotropic lattice dynamics of the BNNTs, which are attributed to the distinct nature of the chemical bonds in the tubular structure. Moreover, the changes in the (002) diffraction positions and intensities suggest that the lattice response of BNNTs to the femtosecond laser excitation involves fast and slow dynamic lattice processes. The fast process, with a time constant of approximately 8 ps, can be understood as a result of electron–phonon coupling, while the slow process, with a time constant of approximately 100 to 300 ps depending on the pumplaser fluence, is ascribed to an Auger recombination effect. In Fig. 3(a), BNNTs were dispersed in ethanol using an ultrasonicator, and a few droplets of a suspension containing BNNTs were cast onto a 2000-mesh Cu grid. In Fig. 3(b), the changes in the (002) diffraction position suggest that the lattice response of the BNNTs to the femtosecond laser excitation involves fast and slow dynamic lattice processes. The bandgap of the BNNTs used here is 5.8 ± 0.3 eV, and the photon energy of our pump laser (wavelength 520 nm) is approximately 2.4 eV. Therefore, three-photon absorption inevitably occurs in the BNNT samples, as schematically shown in Fig. 3(c).

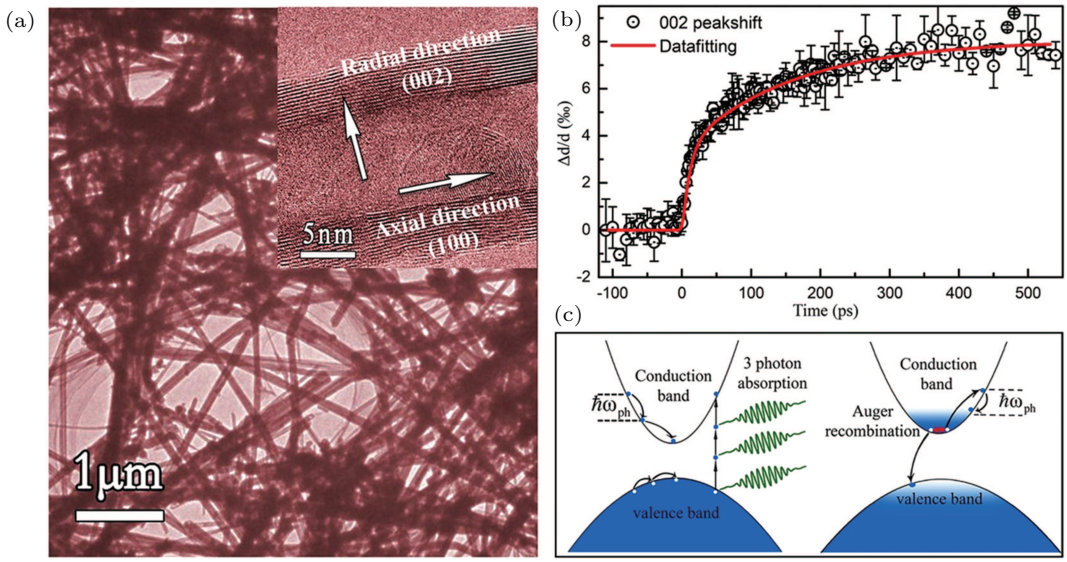


Fig. 3. (color online) Ultrafast structural dynamics of BNNTs. (a) TEM image of the BNNT assemble supported on a Cu grid and a high-resolution lattice image of a single nanotube. (b) Temporal evolution of the (002) peak positions under a pump fluence of 50 mJ/cm^2. The changes in the lattice spacings are fitted with a two-exponential function (red curve). (c) Schematic of the three-photon absorption process following the electron–phonon coupling process and the Auger recombination process causing the secondary phonon-emission process. Reprinted from Ref. [46] with permission.

4.1.2. Optically induced charge density wave transition and dynamic diffraction effects in transition-metal dichalcogenides

Recently, studies employing ultrafast spectroscopy and diffraction (UED, ultrafast x-ray diffraction) have revealed a variety of notable dynamic features in charge density wave (CDW) compounds, including coherently driven collective modes and photoinduced phase transitions. In transition-metal dichalcogenides, experimental observations reveal that photoinduced dynamics often involve multiple transient steps at different timescales.[47,48] The periodic lattice generally undergoes an initial fast decay in a few hundred femtoseconds after optically induced redistribution of the electron density, and then a rapid electron–phonon energy transfer occurs, followed by the recovery of the CDW when the excess energy is redistributed by thermalization.

We recently investigated the optically induced CDW transition of $1T$-$TaSe_2$ from the commensurate phase (C phase, $q_C = 0.225a^* + 0.07b^*$) to the incommensurate phase (IC phase, $q_{IC} = 0.278a^*$) with a visible angular rotation of the CDW wave vector via UTEM investigation, as shown in Figs. 4(a) and (b).[48] Experiments suggest that the photoinduced phase transition in $1T$-$TaSe_2$ contains three transient steps: C-phase suppression, IC-phase growth, and a partial CDW recording from the IC phase to the C phase. The CDW melting and recovery in the C phase can be expressed by $I(t)/I_0 = C_1 \exp(-t/t_1) + C_2[1 - \exp(-t/t_2)]$, where the first term illustrates the CDW melting in the C phase, and the second term represents the recovery of the C phase. The melting of the CDW occurred at the 300–500-fs timescale. Figure 4(c)

clearly shows that a time delay (approximately 2 ps) exists between the C-phase suppression and the IC-phase growth. Moreover, the transition of the superstructure reveals a notable "structural isosbestic point." These results confirm that the nonequilibrium CDW phase transition triggered by photoexcitation often exhibits features different from those observed in the thermal equilibrium transformation.

In ultrafast-diffraction studies, the diffraction-intensity change of the specific Bragg spot often exhibits a notable feature arising from the Debye–Waller effect and coherent oscillations.[7,49] It is believed that a certain anomalous intensity change originates from the zone-axis tilting caused by surface deformation or anisotropic lattice expansion. The dynamic phenomena in metals (Al, Au, and Ag), semimetals (Bi), and semiconductor films (Si) have been extensively reported. Moreover, layered-structure materials often have a far larger thermal expansion coefficient of the c-axis than of the a–b plane, and this anisotropic feature commonly yields a large amplitude-breathing standing wave and anisotropic periodic oscillation in the lattice parameters.[7] We recently reported a series of data on the ultrafast dynamic evolutions observed in 1T-TaSeTe, including the suppression of the satellite spots corresponding to the CDW modulation, the related Debye–Waller effect associated with lattice thermalization, and oscillatory evolutions of the diffraction intensity.[49] According to thin-crystal dynamic diffraction theory, the essential nature of temporal diffraction-intensity alterations is well-explained by anisotropic lattice expansion combined with the Debye–Waller effect.

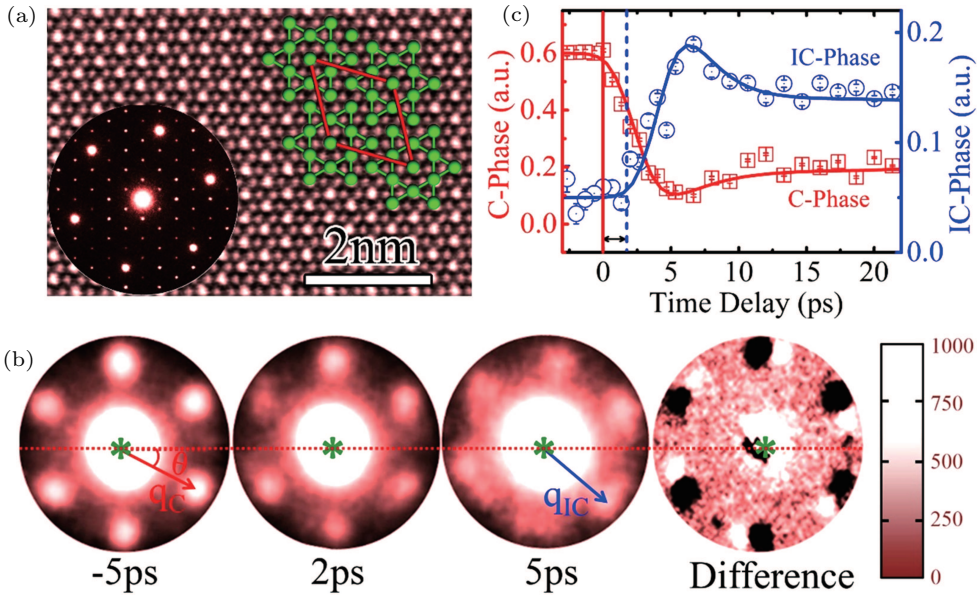


Fig. 4. (color online) Direct observation of an optically induced CDW transition in 1T-$TaSe_2$. (a) High-resolution STEM image and diffraction patterns of CDW modulation in 1T-$TaSe_2$ obtained along the [001] zone-axis direction at room temperature. The inset at the top-right corner shows a schematic of the q_C superstructure. (b) Diffraction patterns for time delays of −5, 2, and 5 ps after ultrafast laser excitation. The rotation of the satellite reflections is visible between −5 and 5 ps. (c) Intensity changes of satellite spots for q_C and q_{IC} as a function of the time delay. Reprinted from Ref. [48] with permission.

4.2. Application of ultrafast imaging techniques of UTEM

In electron diffraction, a high time resolution, up to femtoseconds, is possible, but the data are recorded in the reciprocal space. Ultrafast imaging in the UTEM provides opportunities for studying the elementary processes of structural and morphological changes in real space. Benefiting from state-of-the-art electron optics and the combination of well-developed conventional TEM techniques (BF, DF, HRTEM, LTEM, EFTEM), the UTEM provides the capability of investigating the atomic motion, valence states, magnetic domain, structural domain, structural defects, and strain dynamics in real space with high time and spatial resolutions.[7,26,31,50–59]

The pioneering work regarding the application of ultrafast imaging techniques of the UTEM was performed at Caltech. Zewail *et al.* investigated the structural and morphological changes in single-crystal Au and graphite films using a second-generation ultrafast electron microscope (UEM-2).[13] A variety of dynamic responses to laser pulse excitation were observed, at timescales ranging from picoseconds to microseconds.

Recently, Flannigan *et al.* reported the direct, real-space imaging of the emergence and evolution of acoustic phonons at individual defects in crystalline WSe_2 and Ge via BF imaging with a UTEM. The sub-picosecond nucleation, the launch of wavefronts at step edges, and the resolved dispersion behaviors during propagation and scattering were imaged.[51,52,55] These observations provide unprecedented insight into the roles of the individual atomic and nanoscale features on the

acoustic–phonon dynamics and introduce a new route for the ultraprecise manipulation and control of coherent energy propagation at the atomic scale.

Here, we highlight our recent work to demonstrate the capability of the imaging mode of the UTEM.

4.2.1. Picosecond view of martensitic transition and nucleation in shape-memory alloy

We studied the shape-memory alloy $Mn_{50}Ni_{40}Sn_{10}$ using our home-built UTEM modified from a JEOL-2000EX microscope and reported a picosecond view of a martensitic (MT) transition and nucleation.[59] The experimental results demonstrate that the MT transition and reverse transition in this Heusler alloy contain a variety of structural dynamic features at the picosecond timescale. Imaging and diffraction observations clearly show that the MT transition and MT domain nucleation, which are related to cooperative atomic motions, occur between 10 and 20 ps. Figures 5(a) and 5(b) show a series of ultrafast images illustrating the MT transition and microstructure changes, coupled with a periodic oscillation. It is clearly demonstrated that the annihilation of MT domains (from t_0 to t_1) at ~ 23 ps is due to the photoinduced MT-to-austenitic (AUS) phase transition and that the relaxation time of the oscillation is > 500 ps. Moreover, strong coupling between the MT transition and the lattice breathing mode is discovered in this system, which can result in a periodic structural oscillation between the MT phase and the AUS phase. This allows us to directly observe the MT nucleation and domain-wall motions in transient states using high-spatiotemporal resolution imaging, and provides insights into the elementary mechanisms that govern MT transition. Careful analysis of the ultrafast images and the corresponding electron diffraction patterns reveals the presence of the remarkable transient states, i.e., MT nucleation with a coherent twinning nature, the constraint of the $C4$ symmetry on the growth of the MT nuclei, and the rapid growth of MT plates shown in Figs. 5(c) and 5(d). These results highlight the ability of the UTEM to directly probe the collective atomic motion related to symmetric breaking and to elucidate the mechanisms of domain-wall nucleation in multifunctional materials.

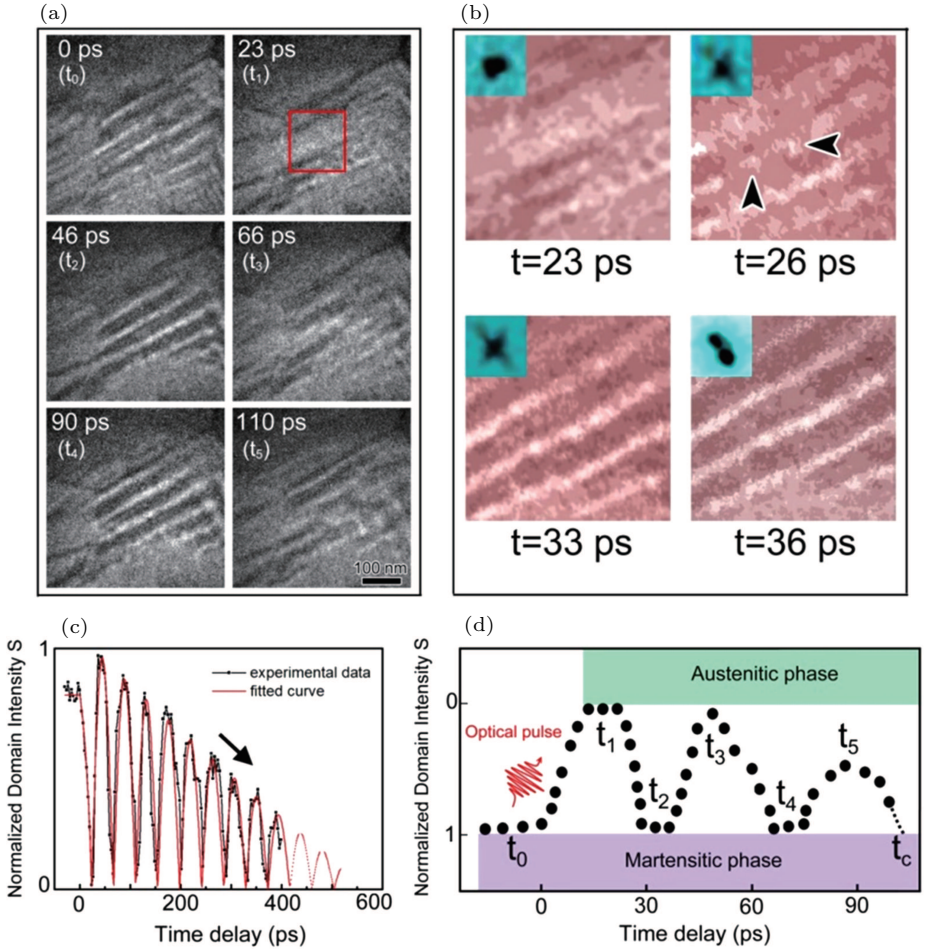


Fig. 5. (color online) Picosecond view of the MT transition and nucleation in the shape-memory alloy $Mn_{50}Ni_{40}Sn_{10}$. (a) Series of ultrafast micrographs showing the periodic annihilation and creation of domains. (b) Structural oscillation obtained from (a), where we clearly observe that the relaxation time of the oscillation is > 500 ps. (c) Careful analysis of the domain nucleation for the boxed area in (a) between $t_1 = 23$ ps and $t_2 = 46$ ps; the presence of tweedlike patterns is evident. The inset of each frame illustrates the progress of the (080) spots, followed by MT domain nucleation. (d) Schematic showing the structural oscillation of $Mn_{50}Ni_{40}Sn_{10}$ due to the strong coupling between the MT transition and the breathing mode. Reprinted from Ref. [59] with permission.

4.2.2. Application of ultrafast imaging techniques to magnetic-dynamics study

LTEM is a powerful technique for performing quantitative analysis of magnetic-domain structures at the sub-50-nm length scale. In a transmission electron microscope, relativistic electrons traversing a thin magnetic sample under an electrostatic field and a magnetic field experience the Lorentz force generated by the sample. If the Lorentz forces acts normal to the travel direction of the electrons, a deflection occurs. Only the in-plane magnetic induction contributes to the deflection. The deflection angle is proportional to the in-plane magnetization and the thickness of the sample. There are two modes in Lorentz microscopy: the Fresnel mode, in which domain walls and magnetization ripples are observed, and the Foucault mode, in which domains are imaged. The LTEM technique evolved from a qualitative magnetic-domain observation technique into a quantitative technique for the determination of the magnetization state of a sample.[60] It has been used to image and analyze complex magnetic textures such as magnetic skyrmions[61] with 2-nm spatial resolution. LTEM has also been applied very successfully to the visualization of flux vortex lattices in Type II superconductors.[62] Recently, by combining ultrafast laser techniques with LTEM, UTEM LTEM has been successfully applied to study ultrafast magnetization dynamics with a high temporal resolution ranging from nanoseconds to picoseconds.[57,58] Zewail *et al.* reported the imaging of the magnetic domain-wall dynamics in a partially oxidized Fe film via the out-of-focus Fresnel method with a nanosecond time resolution.[57] The success of this study demonstrates the promise of the Lorentz UTEM for the real-space imaging of magnetization switching, ferromagnetic resonance, and laser-induced demagnetization in ferromagnetic nanostructures.

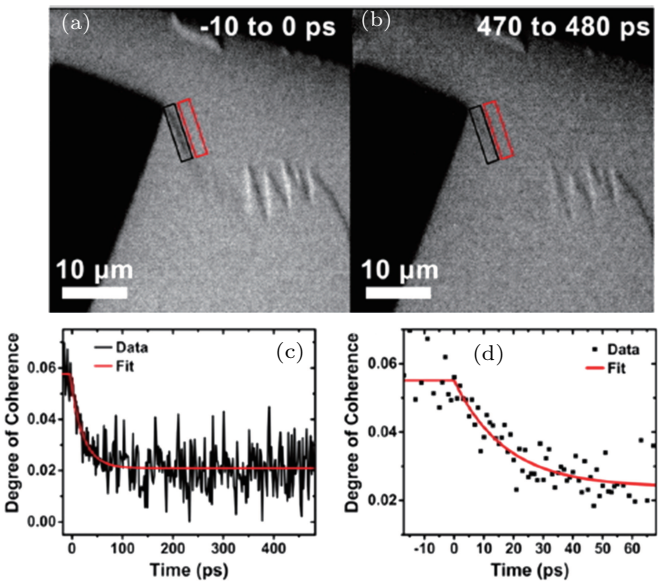


Fig. 6. (color online) Picosecond Fresnel imaging of domain-wall dynamics. (a) Sum of ten separate pulsed-photoelectron Fresnel images obtained before time zero. The black and red rectangles indicate the regions in which the degree of electron coherence was monitored as a function of time. (b) Sum of six separate pulsed photoelectron Fresnel images obtained between 470 and 480 ps (2-ps steps). The same regions indicated in (a) are highlighted. (c) Degree of electron coherence of the domain wall as a function of time. The data range from −18 to 482 ps and present the least-squares fit (red curve) with a single exponential decay having a time constant of 24 ps. (d) Magnified view of the early dynamics data and least-squares fit for the range of −18 to 68 ps. Reprinted from Ref. [58] with permission.

Flannigan *et al.* employed a UTEM for picosecond Fresnel imaging of the photoinduced magnetic-domain wall dynamics in FePt thin films.[58] Under operation with a low instrument repetition rate (5 kHz) and without objective-lens excitation, the picosecond demagnetization of an FePt film was directly imaged via *in situ* femtosecond laser excitation. The dynamics were quantified and monitored according to the time-dependent change in the degree of electron coherence within the magnetic domain walls. Figure 6 shows a series of stroboscopic pump–probe Fresnel images acquired in the experiments, as well as related data analysis.

4.3. Application of ultrafast EELS techniques of UTEM

EELS is a well-established technique for retrieving fundamental information regarding the chemical bonding, electronic structure, and charge distribution at length scales as small as a few nanometers. The low-loss (0–50 eV) region of the spectrum contains electronic information in the form of valence intra- and interband transitions and plasmon excitations. The core-loss (> 100 eV) region of the spectrum contains information regarding the chemical state, local geometric structure, and the nature of chemical bonding centered around the absorbing atom. Particular energy ranges of interest can be chosen by using slits to form energy-filtered images, which is known as EFTEM. The typical energy resolution for TEMs with thermionic field-emission sources is approximately 0.8 eV, and the energy resolution of cold field-emission guns is a few hundred millielectronvolts. A monochromated field-emission electron source can increase the energy resolution to approximately 100 meV by reducing the effects of partial temporal coherence, while the state-of-the-art unique design of the monochromator results in an ultrahigh energy resolution of 10 meV or better (7 meV Nion HERMES 200), which is comparable to phonon energies and other low-energy excitations.[63]

Several UTEM EELS studies have been conducted. Ultrafast core-loss spectroscopy has been demonstrated to probe the electronic and structural dynamics after laser excitation of a graphite nanometer-thin film and C nanotubes, to investigate the coupling between the electronic and lattice motions.[32,64–66] The ability to record at a high resolution (in energy, space, and time) makes it possible to obtain both *in situ* nanoscale elemental and oxidation-state mappings via element-specific imaging.[33,67,68] The value of this methodology is demonstrated by studying the photocatalyst hematite, i.e., α-Fe_2O_3. By employing EFTEM using UTEM equipment, it has been determined that Fe^{4+} ions have a life-

time of a few picoseconds, and the associated photoinduced electronic transitions and charge-transfer processes have been observed.[68]

Here, we demonstrate the capability of UTEM EELS by considering the example of the photoinduced electronic structural dynamics in layered manganite.

4.3.1. Ultrafast electronic dynamics of metallic phase in layered manganite

Bi-layered $PrSr_{0.2}Ca_{1.8}Mn_2O_7$ has a peculiar checkerboard pattern made of ordered orbital stripes originating from the 1:1 ratio of $Mn^{3+}$and Mn^{4+} ions in the ground state. Carbone *et al.* demonstrated coherent structural motions of a $PrSr_{0.2}Ca_{1.8}Mn_2O_7$ single crystal induced by the photoinduced temperature jump, which were detected as periodic modulations of the Bragg peak intensities.[33] Using the same instrument, the resultant modulation of the electron energy-loss function was recorded over a broad energy range (2 to 70 eV), indicating the response of the different electronic states to specific atomic motions.[33] Such an interplay was understood via density functional theory (DFT) calculations of the EEL spectra, in which equilibrated electronic structures for different lattice parameters were obtained, as shown in Fig. 7(a). The overall energy–time map of the experimental data is presented in Fig. 7(b), where the black lines indicate the energies corresponding to the different electronic states observed in the static spectra. Each of these states shows different temporal dynamics, reflecting a different sensitivity to the photoinduced structural distortions. Interestingly, in Fig. 7(c), although the overall effect is the weakest on the Mn M-edge at 53 eV, the periodicity is the clearest at this energy, suggesting that the Mn orbitals are the most sensitive to the structural distortions. This is not surprising, considering the large crystal field on the Mn ions, which we estimated from the band structure and the Mn L-edge static spectrum and is certainly affected by the shape and dimension of the cage surrounding the Mn ions.[33] This study provides the necessary background information to further investigate the more complex regions of the phase diagram and confirms the ability of the ultrafast temperature-modulation approach to provide a direct view of photoinduced thermal phenomena in a solid.

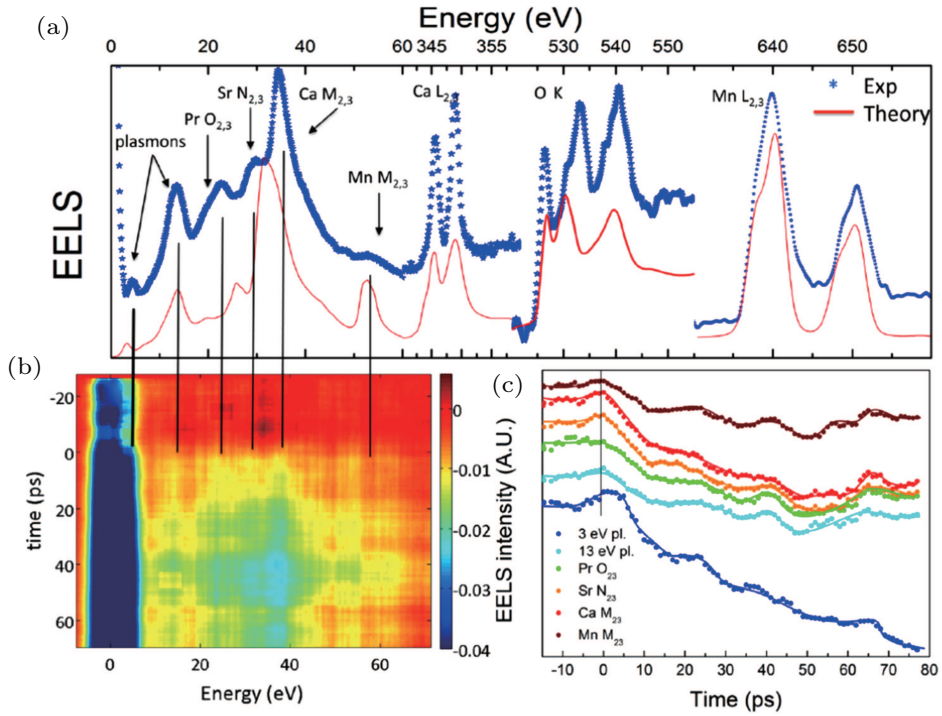


Fig. 7. (color online) Ultrafast electronic dynamics of the metallic phase in the bi-layered $PrSr_{0.2}Ca_{1.8}Mn_2O_7$. (a) Static EELS spectrum from 0 to 700 eV (blue symbols). The red curves indicate theoretical calculations. DFT calculations are used until 600 eV, and atomic multiplet calculations are used for the Mn L-edge above 600 eV. (b) Energy–time map of the low-loss EELS spectrum. The three-dimensional plot is obtained by taking the difference between EELS(t) and EELS($t < 0$). (c) Temporal profile of the EELS intensity at selected energies, which correspond with the specified electronic states. Reprinted from Ref. [33] with permission.

4.4. Application of ultrafast PINEM techniques using UTEM

PINEM was first reported by García De Abajo *et al.* as "electron energy-gain spectroscopy",[69] and was realized by Zewail *et al.* in 2009 using a UTEM.[17] Having a femtosecond time resolution and nanometer spatial resolution, PINEM mainly exploits the absorption and emission of integer photon quanta during the scattering of swift electrons by the field near the boundary or interface of the sample. As an example, figures 8(a) and 8(b) show PINEM results for a C nanotube.[17] If the electrons pass the neighbor of the C nanotube 2 ps before the pump light, we can only detect a single peak near the zero-loss peak of EELS. If the electrons and pump light arrive at the C nanotube simultaneously, we can observe the symmetric

satellite peaks on both sides of the zero-loss EELS peak of the C nanotube, which arise from the absorption of electrons or the emission of photons of integer numbers. An image of the near field near the C nanotube in real space can be obtained using EFTEM.[17]

A high spatial resolution up to 6 nm in PINEM was achieved by Aycan Yurtsever *et al.* in their experimental study involving Ag nanoparticles.[70] In Figs. 8(c)–8(e), the PINEM results for Ag nanoparticles with varied distances are plotted alongside the corresponding electron microscopic images.

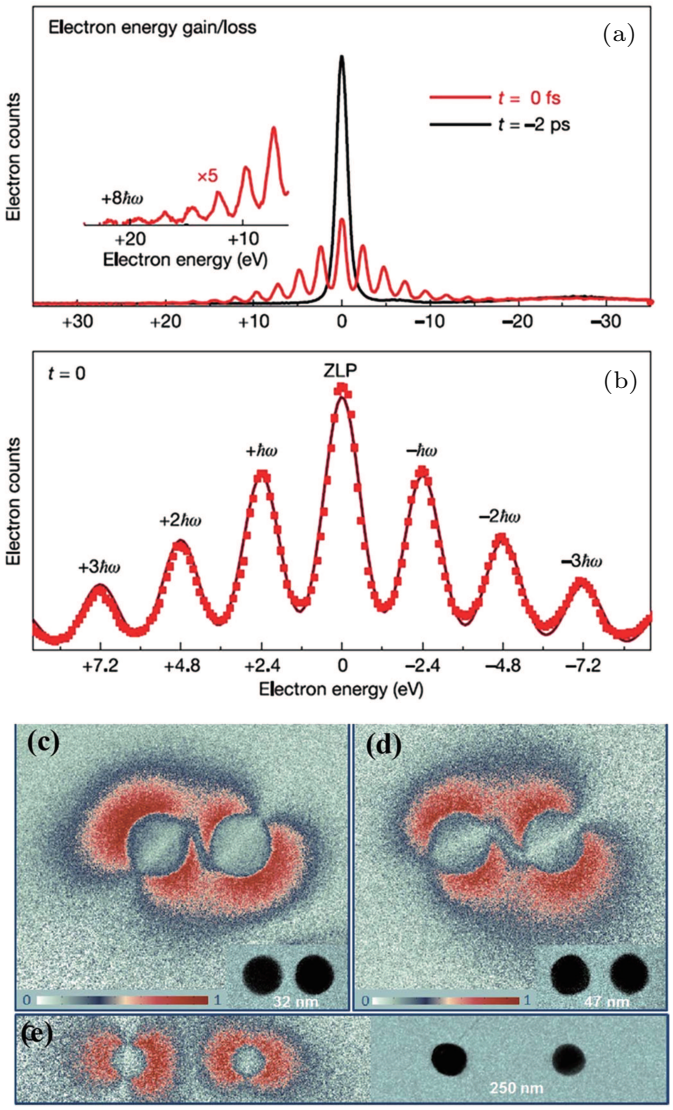


Fig. 8. (color online) (a) Black line indicates the electron-energy spectrum measured when the swift electrons arrive at the C nanotube 2 ps in advance of the pump light. The red line indicates the electron-energy spectrum measured when the swift electrons and pump light arrive at the C nanotube simultaneously. The small inset shows details regarding the energy-gain side of the spectrum, with 5× magnification. (b) Magnified energy spectrum showing the satellite peaks due to the emission and absorption of the near-field photons. (c, d) PINEM and electron microscopic images of pairs of Ag nanoparticles. The distances between the particles are 32, 47, and 250 nm. The directions of the polarization of the excitation laser are different. Polarization of 45° counterclockwise is applied in panels (c) and (d), whereas horizontal polarization is applied in panel (e). Reprinted from Refs. [17] and [70] with permission.

The electric-field distributions around the nanoparticles can be recorded via PINEM. A narrow region with zero field can be visualized when two particles are in close proximity, owing to the entanglement of the dipolar fields, as shown in Figs. 8(c) and 8(d). No such interaction is observed when the Ag nanoparticles are further away from each other (Fig. 8(e)). By solving the Schrödinger equation with the external electromagnetic (EM) field, the position and intensity of the photon absorption and the emission satellite peaks on the two wings of the central zero-loss peak can be well-explained.

PINEM extends the capabilities of the UTEM to the regime of EM-field imaging, and retains the resolution advantage of the UTEM. It is a technology with wide applications in the imaging of photoinduced processes in complex materials, nanostructures, and macromolecules, providing both a direct physical picture of the EM-field distribution and energetic degree-of-freedom information via EELS.[70–77]

5. Outlook

Considered one of the most exciting frontiers in electron microscopy, the field of ultrafast TEM is presently at a pivotal moment in its development. From a technical viewpoint, the greatest challenges that the UTEM faces are to obtain intense high-quality electron pulses and to increase the spatiotemporal resolution. Solutions that have been proposed and are now actively pursued include the development of new emission sources and new schemes for pulse compression, such as a radiofrequency (RF) cavity synchronized to the laser system. To obtain a high brightness of photoelectrons, Ropers *et al.* from the University of Göttingen developed the first UTEM driven by localized photoemission from a field-emitter cathode, which was based on a JEOL JEM-2100 F transmission electron microscope (thermal field emission). Using this UTEM, they achieved record pulse properties in ultrafast electron microscopy with a 9-Å focused beam diameter, a 200-fs pulse duration, and 0.6-eV energy widths, and conducted ultrafast imaging, diffraction, holography, and spectroscopy.[78,79] G. Caruso *et al.* proposed an architecture that allows the introduction of an ultrafast laser beam inside the cold field-emission source of a commercial TEM, aligning and focusing the laser spot on the apex of the nano-emitter.[80] Another method was proposed for realizing ultrafast electron microscopy: RF electron gun-based ultrafast relativistic electron microscopy (Yang Jinfeng; SJ; UCLA).[81] Here, high-energy electrons eliminate the space charge-dominated pulse broadening with sub-100 fs temporal resolution, but this technical scheme is still under development. Recent findings suggest that ultrafast electron microscopy with attosecond-structured wavefunctions may be feasible. Claus Ropers *et al.* introduced a framework for the preparation, coherent manipulation, and characterization

of free-electron quantum states, experimentally demonstrating attosecond electron pulse trains.[82] Peter Baum *et al.* recently demonstrated that the time-resolved diffraction from crystalline Si reveals a <10-as delay of the Bragg emission, demonstrating the possibility of analytic attosecond–ångström diffraction.[83] The combination of attosecond science with electron microscopy can greatly improve the temporal resolution of the UTEM. Furthermore, a direct electron-detection camera has been integrated in the UTEM, which allows for imaging at low repetition rates.[35] As part of the Synergetic Extreme Condition User Facility project of CAS, China, a new UTEM based on the Cs-corrected TEM will be installed in five years in Huairou, Beijing. Meanwhile, a new UTEM based on a cryo-electron microscopy is being installed at the Institute of Physics, CAS.

The UTEM promises to become one of the most powerful experimental tools for the investigation of ultrafast dynamics at the nanoscale, combining a femtosecond temporal resolution with vast capabilities in imaging, diffraction, and spectroscopy. The next-generation UTEM with a field-emission gun and a Cs-corrector can provide a high brightness of the electron source to improve the spatial coherence or increase the spatial resolution for applications such as holography and spatially resolved spectroscopy. From a scientific viewpoint, although various phenomena have been demonstrated using the UTEM—including atomic motions during structural dynamics, transient near-field visualization, phase transitions, carrier transport, biological imaging, cryo-electron microscopy, and biomechanics—systematic research must be performed, and the potential of the UTEM must be explored for various aspects.

References

[1] Chergui M and Zewail A H 2009 *Chemphyschem: A Eur. J. Chem. Phys. Phys. Chem.* **10** 28
[2] Yang L X, Rohde G, Rohwer T, Stange A, Hanff K, Sohrt C, Rettig L, Cortes R, Chen F, Feng D L, Wolf T, Kamble B, Eremin I, Popmintchev T, Murnane M M, Kapteyn H C, Kipp L, Fink J, Bauer M, Bovensiepen U and Rossnagel K 2014 *Phys. Rev. Lett.* **112** 207001
[3] Sun D, Lai J W, Ma J C, Wang Q S and Liu J 2017 *Chin. Phys. B* **26** 037801
[4] Dahms F, Fingerhut B P, Nibbering E T J, Pines E and Elsaesser T 2017 *Science* **357** 491
[5] Bostedt C, Boutet S, Fritz D M, Huang Z R, Lee H J, Lemke H T, Robert A, Schlotter W F, Turner J J and Williams G J 2016 *Rev. Mod. Phys.* **88** 015007
[6] Rettig L, Mariager S O, Ferrer A, Grubel S, Johnson J A, Rittmann J, Wolf T, Johnson S L, Ingold G, Beaud P and Staub U 2015 *Phys. Rev. Lett.* **114** 067402
[7] Zewail A H 2009 *4D Electron Microscopy Imaging in Space and Time* (Imperial College Press)
[8] Domer H and Bostanjoglo O 2003 *Rev. Sci. Instrum.* **74** 4369
[9] Zewail A H 2010 *Science* **328** 187
[10] Browning N D, Bonds M A, Campbell G H, Evans J E, LaGrange T, Jungjohann K L, Masiel D J, McKeown J, Mehraeen S, Reed B W and Santala M 2012 *Curr. Opinion Solid State Mater. Sci.* **16** 23
[11] Cao G L, Sun S S, Li Z W, Tian H F, Yang H X and Li J Q 2015 *Sci. Rep.-Uk* **5** 8404
[12] Park H S, Baskin J S, Kwon O H and Zewail A H 2007 *Nano Lett.* **7** 2545
[13] Brett Barwick H S P, Oh-Hoon Kwon, J Spencer Baskin and Ahmed H Zewail 2008 *Science* 1227
[14] Bostanjoglo O 2002 *Adv. Imaging Electron. Phys.* **121** 1
[15] Hassan M T, Baskin J S, Liao B and Zewail A H 2017 *Nat. Photon.* **11** 425
[16] Shorokhov D and Zewail A H 2009 *J. Am. Chem. Soc.* **131** 17998
[17] Barwick B, Flannigan D J and Zewail A H 2009 *Nature* **462** 902
[18] Batson P E 2011 *Proc. Natl. Academy Sci. United States Am.* **108** 3099
[19] Flannigan D J, Barwick B and Zewail A H 2010 *Proc. Natl. Academy Sci. United States Am.* **107** 9933
[20] Flannigan D J, Park S T and Zewail A H 2010 *Nano Lett.* **10** 4767
[21] King W E, Campbell G H, Frank A, Reed B, Schmerge J F, Siwick B J, Stuart B C and Weber P M 2005 *J. Appl. Phys.* **97** 111101
[22] Lobastov V A, Srinivasan R and Zewail A H 2005 *Proc. Natl. Academy Sci. United States Am.* **102** 7069
[23] Miller R J, Ernstorfer R, Harb M, Gao M, Hebeisen C T, Jean-Ruel H, Lu C, Moriena G and Sciaini G 2010 *Acta Crystallogr. Sect. A: Found. Crystallogr.* **66** 137
[24] Shorokhov D and Zewail A H 2008 *Phys. Chem. Chem. Phys.: PCCP* **10** 2879
[25] Thomas J M 2005 *Angew. Chem.* **44** 5563
[26] Vanacore G M, Fitzpatrick A W P and Zewail A H 2016 *Nano Today* **11** 228
[27] Zewail A H 2006 *Annu. Rev. Phys. Chem.* **57** 65
[28] Zewail A H 2010 *Philos. Trans. Ser. A: Math. Phys. Eng. Sci.* **368** 1191
[29] Ziegler A 2011 *MRS Bull.* **36** 121
[30] Carbone F 2011 *Eur. Phys. J.-Appl. Phys.* **54** 33503
[31] Plemmons D A, Suri P K and Flannigan D J 2015 *Chem. Mater.* **27** 3178
[32] Carbone F 2010 *Chem. Phys. Lett.* **496** 291
[33] Piazza L, Ma C, Yang H X, Mann A, Zhu Y, Li J Q and Carbone F 2014 *Structural Dyn.* **1** 014501
[34] Bucker K, Picher M, Cregut O, LaGrange T, Reed B W, Park S T, Masiel D J and Banhart F 2016 *Ultramicroscopy* **171** 8
[35] Lee Y M, Kim Y J, Kim Y J and Kwon O H 2017 *Structural Dyn.* **4** 044023
[36] Ji S, Piazza L, Cao G, Park S T, Reed B W, Masiel D J and Weissenrieder J 2017 *Structural Dyn.* **4** 054303
[37] Andreev S V, Aseev S A, Bagratashvili V N, Vorob'ev N S, Ishchenko A A, Kompanets V O, Malinovskii A L, Mironov B N, Timofeev A A, Chekalin S V, Shashkov E V and Ryabov E A 2017 *Quantum Electron* **47** 116
[38] Kieft E, Schliep K B, Suri P K and Flannigan D J 2015 *Structural Dyn.* **2** 051101
[39] Petruk A A, Pichugin K and Sciaini G 2017 *Structural Dyn.* **4** 044005
[40] Plemmons D A and Flannigan D J 2017 *Chem. Phys. Lett.* **683** 186
[41] Piazza L, Masiel D J, LaGrange T, Reed B W, Barwick B and Carbone F 2013 *Chem. Phys.* **423** 79
[42] Yurtsever A and Zewail A H 2009 *Science* **326** 708
[43] Park S T, Flannigan D J and Zewail A H 2011 *J. Am. Chem. Soc.* **133** 1730
[44] Park S T, Flannigan D J and Zewail A H 2012 *J. Am. Chem. Soc.* **134** 9146
[45] Grinolds M S, Lobastov V A, Weissenrieder J and Zewail A H 2006 *Proc. Natl. Academy Sci. United States Am.* **103** 18427
[46] Li Z W, Sun S S, Li Z A, Zhang M, Cao G L, Tian H F, Yang H X and Li J Q 2017 *Nanoscale* **9** 13313
[47] Eichberger M, Schafer H, Krumova M, Beyer M, Demsar J, Berger H, Moriena G, Sciaini G and Miller R J D 2010 *Nature* **468** 799
[48] Sun S S, Wei L L, Li Z W, Cao G L, Liu Y, Lu W J, Sun Y P, Tian H F, Yang H X and Li J Q 2015 *Phys. Rev. B* **92** 224303
[49] Wei L L, Sun S S, Guo C, Li Z W, Sun K, Liu Y, Lu W J, Sun Y P, Tian H F, Yang H X and Li J Q 2017 *Structural Dyn.* **4** 044012
[50] Campbell G H, LaGrange T, Kim J S, Reed B W and Browning N D 2010 *J. Electron. Microscopy* 59 Suppl **1** S67
[51] Cremons D R, Du D X and Flannigan D J 2017 *Phys. Rev. Mater.* **1** 073801
[52] Cremons D R, Plemmons D A and Flannigan D J 2016 *Nat. Commun.* **7** 11230
[53] Flannigan D J and Zewail A H 2010 *Nano Lett.* **10** 1892
[54] Kwon O H , Park H S, Baskin J S and Zewail A H 2010 *Nano Lett.* **10** 3190

[55] McKenna A J, Eliason J K and Flannigan D J 2017 *Nano Lett.* **17** 3952
[56] Park H S, Baskin J S, Barwick B, Kwon O H and Zewail A H 2009 *Ultramicroscopy* **110** 7
[57] Park H S, Baskin J S and Zewail A H 2010 *Nano Lett.* **10** 3796
[58] Schliep K B, Quarterman P, Wang J P and Flannigan D J 2017 *Appl. Phys. Lett.* **110** 222404
[59] Zhang M, Cao G, Tian H, Sun S, Li Z, Li X, Guo C, Li Z, Yang H and Li J 2017 *Phys. Rev. B* **96** 174203
[60] McVitie S and Cushley M 2006 *Ultramicroscopy* **106** 423
[61] Yu X Z, Onose Y, Kanazawa N, Park J H, Han J H, Matsui Y, Nagaosa N and Tokura Y 2010 *Nature* **465** 901
[62] Loudon J C, Yazdi S, Kasama T, Zhigadlo N D and Karpinski J 2015 *Phys. Rev. B* **91** 054505
[63] Mukai M, Okunishi E, Ashino M, Omoto K, Fukuda T, Ikeda A, Somehara K, Kaneyama T, Saitoh T, Hirayama T and Ikuhara Y 2015 *Microscopy-Jpn.* **64** 151
[64] Carbone F, Kwon O H and Zewail A H 2009 *Science* **325** 181
[65] Vanacore G M, van der Veen R M and Zewail A H 2015 *ACS Nano* **9** 1721
[66] van der Veen R M, Penfold T J and Zewail A H 2015 *Structural Dyn.* **2** 024302
[67] Ortalan V and Zewail A H 2011 *J. Am. Chem. Soc.* **133** 10732
[68] Su Z, Baskin J S, Zhou W, Thomas J M and Zewail A H 2017 *J. Am. Chem. Soc.* **139** 4916
[69] Asenjo-Garcia A and García de Abajo F J 2013 *New J. Phys.* **15** 103021
[70] Yurtsever A, Baskin J S and Zewail A H 2012 *Nano Lett.* **12** 5027
[71] Yurtsever A and Zewail A H 2012 *Nano Lett.* **12** 3334
[72] Ryabov A and Baum P 2016 *Science* **353** 374
[73] Park S T, Yurtsever A, Baskin J S and Zewail A H 2013 *Proc. Natl. Academy Sci. United States Am.* **110** 9277
[74] Lummen T T, Lamb R J, Berruto G, LaGrange T, Dal Negro L, Garcia de Abajo F J, McGrouther D, Barwick B and Carbone F 2016 *Nat. Commun.* **7** 13156
[75] Barwick B and Zewail A H 2015 *ACS Photon.* **2** 1391
[76] Feist A, Echternkamp K E, Schauss J, Yalunin S V, Schafer S and Ropers C 2015 *Nature* **521** 200
[77] Piazza L, Lummen T T, Quinonez E, Murooka Y, Reed B W, Barwick B and Carbone F 2015 *Nat. Commun.* **6** 6407
[78] Storeck G, Vogelgesang S, Sivis M, Schafer S and Ropers C 2017 *Structural Dyn.* **4** 044024
[79] Feist A, Bach N, Rubiano da Silva N, Danz T, Moller M, Priebe K E, Domrose T, Gatzmann J G, Rost S, Schauss J, Strauch S, Bormann R, Sivis M, Schafer S and Ropers C 2017 *Ultramicroscopy* **176** 63
[80] Caruso G M, Houdellier F, Abeilhou P and Arbouet A 2017 *Appl. Phys. Lett.* **111** 023101
[81] Yang J, Yoshida Y and Shibata H 2015 *Electron. Commun. Jpn.* **98** 50
[82] Priebe K E, Rathje C, Yalunin S V, Hohage T, Feist A, Schaer S and Ropers C 2017 *Nat. Photon.* **11** 793
[83] Morimoto Y and Baum P 2018 *Nat. Phys.* **14** 252